

Tunable THz Graphene Plasmonic Filter Based on One-Dimensional Photonic Quasicrystals

YIBING ZHONG^a, YINSHAN YU^{b,*}, SHENGLI SHI^a,
MINGXING GAO^a, YUHAO WANG^a AND CHUNYAN LV^a

^a*Shandong Institute of Space Electronic Technology, China Academy of Space Technology,
Yantai 264670, China*

^b*Faculty of Electronic Information Engineering, Huaiyin Institute of Technology,
Huai'an 223003, China*

Received: 04.12.2019 & Accepted: 17.08.2020

Doi: [10.12693/APhysPolA.138.763](https://doi.org/10.12693/APhysPolA.138.763)

*e-mail: yuyinshan@hyit.edu.cn

In this paper, a tunable multichannel THz graphene plasmonic filter based on a one-dimensional Fibonacci photonic quasicrystal is proposed. The filter properties of this integrated plasmonic device are investigated theoretically by applying the transfer matrix method in numerical calculation. The transmission spectrum can be flexibly tuned via a varying Fibonacci generation order, the chemical potential of graphene and the thickness of the multilayer stacks of photonic quasicrystals. Furthermore, the spectrum property of the proposed structure is sensitive to the refractive index of the dielectric layers. The well-performed plasmonic filter paves the new way for designing THz on-chip graphene devices.

topics: filter, graphene plasmonics, Fibonacci photonic quasicrystals, THz

1. Introduction

Graphene is an allotrope of carbon in the form of a two-dimensional, atomic-scale, honey-comb lattice in which one atom forms each vertex. It was originally observed in electron microscopes in 1962 and rediscovered, isolated and characterized in 2004 by Andre Geim and Konstantin Novoselov [1, 2]. It has attracted extensive research for the last fifteen years because of its unique electrical [3] and optical properties [4, 5]. The intriguing features of graphene are mainly exhibited in high carrier mobility [3], dynamic tunability [6], constant light absorption [7] and low losses [8]. These unprecedented characteristics of the atom-thick 2D material make graphene a promising candidate for integrated optical devices, such as enhanced absorbers [9], multichannel filters [10], optical biosensors [11], magneto-optic modulators [12, 13], photodetectors [14] and optical polarizers [15]. Graphene can support surface plasmon polaritons (SPPs) in the THz frequency range which is also called graphene plasmonics (GPs) [16]. When compared to traditional metal-based plasmonics mainly generated in the visible and near-infrared region [17], GPs have shown better performance in the THz frequency range for their strong optical field confinement [4], longer propagation length [16] and flexible chemical or electrostatic tunability [18, 19]. Moreover, researchers have proved that graphene is capable of supporting both the TM-polarization

and TE-polarization SPPs [20] which shows more potential applications and benefits in comparison with the noble metals only supporting the TM modes. With the abundance of research focused on GPs, plenty of graphene-based plasmonic proposals have been put forward, such as a directional coupler [21], rainbow trapping [22] and graphene modulator [23]. All these devices show that this special 2D optical material has a bright future ahead in the field of integrated photonic facilities which needs further and deeper investigations.

One-dimensional photonic crystals (PCs) are multilayer structures made up of two alternative dielectrics with different refractive indexes. Similar to electronic semiconductors showing electron band gaps in their band structure, PCs show photonic band gaps (PBGs) in their corresponding frequency region which is known as the Bragg condition [24]. Namely, PCs can allow or prohibit the propagation of electromagnetic waves in the multilayer structures for incident waves with different frequencies. With comprehensive investigations relating to PCs, a complete theory model and experiment demonstrations have been established [24]. Moreover, researchers have designed plenty of useful devices related to PCs, such as high-quality filters [25, 26], absorbers [27, 28] and photonic waveguides [29]. Recently, endeavors have been made to explore various transmission spectra of photonic crystals but the spectra of the conventional periodic one-dimensional photonic crystals

generally do not easily generate multiple PBGs in a specific frequency range. Hence, resorting to quasiperiodic photonic crystals (QPPCs) seems to be a reasonable solution to get a rich spectrum and multiple PBGs. The idea of photonics in quasiperiodic structures was first proposed by Kohmoto in 1987 by introducing the Fibonacci sequence into multilayer structures [30]. The field of photonic quasicrystals has thrived for more than the last thirty years [31–33]. It is still one of the most vital areas in the field of photonic crystals due to its intriguing properties. Generally, photonic quasicrystals indicate deterministic aperiodic photonic crystal structures following substitution rules [32], such as the Fibonacci sequence, Cantor sequence and Thue-Morse sequence in the one-dimensional case. The so-called substitution rules are defined by replacing a group of letter series “A” representing a combination of dielectric materials stacks $\{\dots, A, B, C, \dots\}$ with a different letter sequence “ \bar{A} ” denoting the other combination of block materials. By iterating the substitution rules originating from the group “ \bar{A} ” set, different determined aperiodic strings can be generated corresponding to several generation orders. By this means, a diversity of an aperiodic photonic structure has been proposed with different applications in research and engineering. For example, the well-known Fibonacci quasiperiodic sequence follows the substitution rule “ $A \rightarrow AB, B \rightarrow A$ ”, where A and B denote different dielectric material layers. As the layer number of a corresponding sequence order F_j follows the Fibonacci number, this kind of photonic quasicrystals is also named the Fibonacci sequence. Quasiperiodic structures adhering to substitution rules show multiple band gaps and self-similar patterns in their transmission spectrum. These structures have shown many potential applications on various occasions [34, 35].

Generally, the transfer matrix method is widely used in analyzing photonic crystals. In 2016, S. Bin et al. demonstrated that photonic crystals covered by a single layer graphene can be treated as graphene plasmonic crystals. Thus, the transfer matrix method is also applicable in graphene coated grating structure [6]. Then, Y.C. Feng et al. and D.F. Zhou et al. applied a quasiperiodic sequence such as the Fibonacci sequence [10] and the arithmetic sequence [36] in similar structures which show a multiple filter performance. However, the dispersion relationship of graphene plasmonics in the former three-layer structure is rather complicated and hard to be calculated. In this paper, we show that the dispersion relationship of the plasmonic structures can be simplified when the layer thickness exceeds 100 nm and the multiple filter property is still maintained. The proposed tunable multichannel THz graphene plasmonic filter is composed of a one-dimensional photonic quasicrystal with monolayer graphene covered on the top of

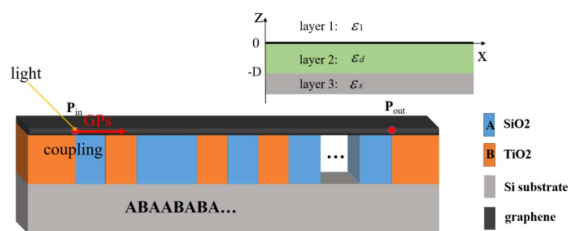


Fig. 1. The schematic diagram of the proposed quasiperiodic plasmonic filter following the Fibonacci sequence. Light couples in at the point P_{in} and the transmission properties are computed at P_{out} point. The inset on the upper panel demonstrates a simplified model for calculating the dispersion relationship for GPs propagating along graphene.

it, as shown in Fig. 1. The simplified schematic diagram of the dielectric-graphene-dielectric-substrate (DGDS) structure is shown in the upper panel of Fig. 1. The multilayer structures are alternative dielectric layers SiO_2 (A) and TiO_2 (B) which are grown on the silicon substrate. These dielectric materials are traditional optical materials used in many types of researches. In calculation, we take the refractive index of SiO_2 and TiO_2 as 1.45 and 2.13 [37], respectively. According to the effective index theory [6], PCs propagating graphene plasmonics can be regarded as plasmonic crystals, therefore, the calculation method that applies to general PCs also applies to graphene-based plasmonic crystals. Based on Maxwell’s equations, we calculated the dispersion relationship of the proposed structure by applying different boundary conditions in different interfaces. The transmission properties of the filter are derived by the transfer matrix method (TMM) in simulation. Moreover, we calculate the transmission properties of different generation order of the Fibonacci sequence. The tunable properties are discussed for various graphene chemical potentials and multilayer thickness. Finally, the influence of the dielectric refractive index on the filter performance is also investigated. The proposed structure of the GPs filter possesses highly flexible tunability and is sensitive to parameter changes. Therefore, the idea of introducing the quasiperiodic sequence may be helpful in designing optical-electrical devices such as absorbers, sensors and filters.

2. Theory model

The photonic crystal was grown on a silicon substrate with a monolayer graphene covered on the top of it, as shown in Fig. 1. The quasiperiodic order of PCs is arranged in the Fibonacci sequence as ABAABABA... The inset of Fig. 1 is the simplified schematic diagram of the dielectric-graphene-dielectric-substrate (DGDS) model and the thickness of the alternative materials between graphene and substrate is D .

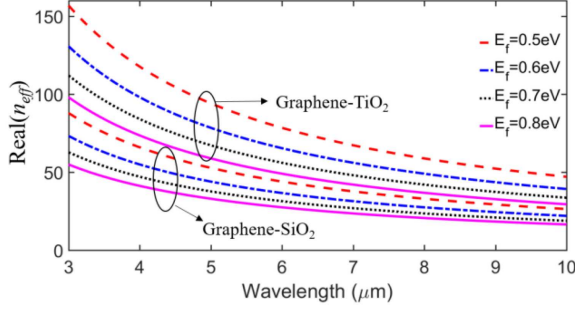


Fig. 2. Dispersion relationship of air/graphene/SiO₂ and air/graphene/TiO₂ structures for different chemical potentials in the THz regime.

The dispersion relation of the GPs propagating along the x -axis between the graphene sheet and the underlying dielectrics can be derived by applying boundary conditions into Maxwell's equations. Referring to the inset of Fig. 1, the spatial distribution of the dielectric constant is:

$$\varepsilon(z) = \begin{cases} \varepsilon_1, & z > 0 \\ \varepsilon_d, & -D < z < 0 \\ \varepsilon_s, & z < -D \end{cases} \quad (1)$$

where ε_1 and ε_s denote the permittivity of the upper and substrate dielectric materials and ε_d indicates the permittivity of the dielectric A or B, with respect to ε_{d1} and ε_{d2} . According to Maxwell's electromagnetic theory, for a TM-mode case, the \mathbf{H} and \mathbf{E} field component in each layer of the DGDS structure can be expressed in the form:

$$H_{1y} = H_1 \exp(-k_1 z + i\beta x), \quad (2)$$

$$E_{1x} = i \frac{k_1 H_1}{\omega \varepsilon_0 \varepsilon_1} \exp(-k_1 z + i\beta x), \quad (3)$$

$$E_{1z} = -\frac{\beta H_1}{\omega \varepsilon_0 \varepsilon_1} \exp(-k_1 z + i\beta x), \quad (4)$$

in layer 1 ($z > 0$), while

$$H_{2y} = [H_{21} e^{-k_2 z} + H_{22} e^{k_2 z}] e^{i\beta x}, \quad (5)$$

$$E_{2x} = i \frac{k_2}{\omega \varepsilon_0 \varepsilon_d} (H_{21} e^{-k_2 z} + H_{22} e^{k_2 z}) e^{i\beta x}, \quad (6)$$

$$E_{2z} = -\frac{\beta}{\omega \varepsilon_0 \varepsilon_d} (H_{21} e^{-k_2 z} + H_{22} e^{k_2 z}) e^{i\beta x} \quad (7)$$

in layer 2 ($-D < z < 0$). Similarly, in layer 3 ($z < -D$), we may have:

$$H_{3y} = H_3 \exp(k_3 z + i\beta x), \quad (8)$$

$$E_{3x} = i \frac{k_3 H_3}{\omega \varepsilon_0 \varepsilon_s} \exp(k_3 z + i\beta x), \quad (9)$$

$$E_{3z} = -\frac{\beta H_3}{\omega \varepsilon_0 \varepsilon_s} \exp(k_3 z + i\beta x). \quad (10)$$

Here, $k_i = \sqrt{\beta^2 - \varepsilon_i k_0^2}$ [38] is the attenuation coefficients of the surface wave in the normal direction z of the interface in layer i . The wave vector along the propagation direction x is denoted as

$\beta = n_{\text{eff}} k_0$, n_{eff} and $k_0 = \omega/c$ is the effective refractive index and free-space wave vector, in which ω is the angular frequency of photon and c is the speed of light in vacuum. With monolayer graphene lying between layer 1 and layer 2, the boundary conditions at the interface $z = 0$ can be expressed as:

$$E_{1x} = E_{2x}, \quad H_{1y} - H_{2y} = \sigma E_{1x}, \quad (11)$$

where σ is the conductivity of the graphene layer. At the interface $z = -D$:

$$E_{2x} = E_{3x}, \quad H_{2y} = H_{3y}. \quad (12)$$

Hence, the dispersion relationship of the DGDS structure can be obtained in the following way [10, 38]:

$$\left(\frac{\varepsilon_d}{k_d} + \frac{\varepsilon_{\text{sub}}}{k_{\text{sub}}} \right) \left(\frac{\varepsilon_d}{k_d} + \frac{\varepsilon_1}{k_1} + i \frac{\sigma}{\omega \varepsilon_0} \right) = \left(\frac{\varepsilon_d}{k_d} - \frac{\varepsilon_{\text{sub}}}{k_{\text{sub}}} \right) \left(\frac{\varepsilon_d}{k_d} - \frac{\varepsilon_1}{k_1} - i \frac{\sigma}{\omega \varepsilon_0} \right) e^{-2k_d D}. \quad (13)$$

In the THz region, the propagation constant $\beta \gg k_0$ (see Fig. 2) and (13) can be simplified to [39, 40]:

$$\frac{2\varepsilon_1}{\beta} = -i \frac{\sigma}{\omega \varepsilon_0} \left(1 - \frac{\varepsilon_1 - \varepsilon_s}{\varepsilon_1 + \varepsilon_s} e^{-2\beta D} \right). \quad (14)$$

Note that (14) is the exact form of the dispersion relation for the proposed structure in Fig. 1. With a simple derivation, one can even write that

$$\beta = i \frac{\omega \varepsilon_0}{\sigma} \frac{(\varepsilon_d + \varepsilon_1) - \frac{(\varepsilon_d - \varepsilon_{\text{sub}})(\varepsilon_d - \varepsilon_1)}{\varepsilon_d + \varepsilon_{\text{sub}}} e^{-2\beta D}}{1 + \frac{\varepsilon_d - \varepsilon_{\text{sub}}}{\varepsilon_d + \varepsilon_{\text{sub}}} e^{-2\beta D}}. \quad (15)$$

Clearly, larger dielectric thickness D would reduce the effect of the substrate on the dispersion relationship (as D tending to ∞ means no substrate) which is consistent with our intuitive speculation. The value of β is $\approx 50k_0$ in our calculation (Fig. 2), thus the term $e^{-2\beta D}$ can be neglected when $D > 100$ nm. When $e^{-2\beta D}$ tends to 0, so (15) takes the form:

$$\beta = \frac{i\omega \varepsilon_0}{\sigma} (\varepsilon_1 + \varepsilon_d). \quad (16)$$

In the real experiment, the layer thickness is easy to be achieved to $D < 100$ nm by vapor deposition and the substrate material will have little influence on the performance of the proposed device. Furthermore, we will address the other limitation for the layer thickness $D < 50$ μm because the optical chips made in cleanroom are generally in this scale. Therefore, in the following discussion, we will consider the DGDS structure without the substrate layer and all the dielectric thickness d_A (d_B) is chosen within the range of $100 \text{ nm} < D < 50 \mu\text{m}$ in calculation. The conductivity of graphene can be expressed by the Kubo formula [41]:

$$\sigma = i \frac{e^2}{4\pi\hbar} \ln \left(\frac{2|\mu_c| - \hbar\omega + i\hbar\tau^{-1}}{2|\mu_c| + \hbar\omega + i\hbar\tau^{-1}} \right) + \frac{i e^2 k_B T}{\pi \hbar^2 (\omega + i\tau^{-1})} \left[\frac{\mu_c}{k_B T} + 2 \ln \left(e^{\mu_c/(k_B T)} + 1 \right) \right]. \quad (17)$$

Here, e is the electron charge, k_B is the Boltzmann constant, T is the temperature, \hbar is the reduced

Planck constant, $\tau = \mu\mu_C/(ev_f^2)$ is the momentum relaxation time of the electron, μ stands for electron mobility at a range of 10000 to 40000 $\text{cm}^2/(\text{V s})$, $v_f = 10^6$ m/s is the Fermi velocity and μ_C represents the chemical potential (which is also called the Fermi energy) of graphene. The chemical potential μ_C can be modulated by many external conditions, such as gate voltage, magnetic field and chemical doping. This intriguing property introduces much degree of freedom when designing optical integrated circuit devices. In (17), the former term corresponds to the intraband electron-photon scattering process while the latter term corresponds to the direct interband electron transition. In the THz region, the intraband process contribution dominates while the interband process contributes little to conductivity. Therefore, (17) can be simplified to:

$$\sigma = i \frac{e^2\mu_C}{\pi\hbar^2(\omega + i\tau^{-1})}. \quad (18)$$

Based on the dispersion relationship of the DGDS structure, we can compute the effective index of air/graphene/silica and air/graphene/titanium oxide structure as $n_{\text{eff,A}}$ and $n_{\text{eff,B}}$, respectively, where $n_{\text{eff,A,B}} = \beta_{\text{A,B}}/k_0$. All materials are assumed as nonmagnetic here. A Fibonacci quasiperiodic structure is based on the Fibonacci sequence and the sequence expression is given by substitution rule “A \rightarrow AB, B \rightarrow A”. The expression can be given by $S_0 = \{\text{B}\}$ and $S_1 = \{\text{A}\}$, so that $S_2 = \{\text{AB}\}$, $S_3 = \{\text{ABA}\}$, $S_4 = \{\text{ABAAB}\}$ and $S_5 = \{\text{ABAABABA}\}$, $S_6 = \{\text{ABAABABAABAAB}\}$ and so on. Figure 1 shows the structure of one-dimensional Fibonacci photonic crystal of the generation order S_5 with thickness d_A and d_B .

We use the well-known transfer matrix method (TMM) to obtain the optical properties of the proposed structure and the characteristic matrix M_i ($i = \text{A, B}$) of a single block is calculated by [42]:

$$M_i = \begin{pmatrix} \cos(\beta_i d_i) & -i q_i^{-1} \sin(\beta_i d_i) \\ i q_i \sin(\beta_i d_i) & \cos(\beta_i d_i) \end{pmatrix} \quad (19)$$

for the TM polarization wave, $\beta_i = k_0 n_{\text{eff},i}$ and $q_i = 1/n_{\text{eff},i}$ ($i = \text{A, B}$). The total characteristic matrix of the entire structure would be:

$$M_t = \prod_j M_j = \begin{pmatrix} M_{11} & M_{12} \\ M_{21} & M_{22} \end{pmatrix}, \quad (20)$$

where $j = \text{A, B}$ corresponds to the particular layer index. For example, the characteristic matrix for the one-dimensional Fibonacci photonic crystal with the generation order S_5 is presented by $M_5 = M_A M_B M_A M_A M_B M_A M_B M_A$. The transmission coefficient of the GPs on the FPCG structure can be calculated using

$$t = \frac{2p_1}{(M_{11} + M_{12}p_L)p_1 + (M_{21} + M_{22}p_L)}, \quad (21)$$

where $p_1 = \sqrt{\mu_1/\varepsilon_L}$ are the external ambient parameters of the incident and exit port P_{in} and P_{out} . In this article, we mainly focus on the TM mode.

3. Results and discussion

Figure 2 shows the real part of the effective refractive index n_{eff} for air/graphene/SiO₂ structure and air/graphene/TiO₂ structure with different graphene chemical potential μ_C according to (16). In this plot, the red dashed line stands for the chemical potential $\mu_C = 0.5$ eV, the blue dot-dashed line — for $\mu_C = 0.6$ eV, the black dotted line — for $\mu_C = 0.7$ eV and the magenta solid line for $\mu_C = 0.8$ eV. As we can see in the picture, for a given graphene chemical potential μ_C , the effective refractive index of GPs propagating in the interface of air/graphene/TiO₂ structure is much larger than that of the air/graphene/SiO₂ structure. This result can be referred to the dispersion relationship in (16) as n_{SiO_2} is smaller than n_{TiO_2} for a particular wavelength. In a specific structure (i.e., air/graphene/SiO₂ or air/graphene/TiO₂), it is clear that with the increment of the graphene chemical potential, the real part of the effective refractive index of GPs decreases. The reason for this tendency comes from (18). Obviously, the conductivity of graphene is proportional to the chemical potential. Therefore, the effective refractive index is inversely proportional to the chemical potential according to (16). In a general case, the chemical potential of graphene can be tuned by applying biased gate voltage V_g on monolayer graphene and the deterministic relation of the chemical potential μ_C can be given by $\mu_C = \hbar v_f \sqrt{\pi n}$ and $n = \varepsilon_d \varepsilon_0 v_g / (ed)$ is the charge density of a graphene layer [1, 6]. The transform of the effective refractive index of the DGDS structure for different chemical potential μ_C demonstrates that the proposed photonic device is indeed tunable by varying gate voltages.

The transmission spectrum is depicted in Fig. 3 for various generation orders S_j of the Fibonacci sequence in the THz regime. Multiple PBGs are obtained for different Fibonacci orders due to the intrinsic property of the Fibonacci structure which is similar to previous papers [10, 30]. The chemical potential of graphene is fixed to $\mu_C = 0.7$ eV, with a layer thickness of alternative blocks chosen as (a) $d_A = 50$ nm, $d_B = 60$ nm and (b) $d_A = 60$ nm, $d_B = 50$ nm. We can find three well-performed band gaps located at 35 THz, 58 THz and 78 THz in Fig. 3a and five band gaps located at 35 THz, 46 THz, 58 THz, 68 THz and 78 THz in Fig. 3b. Clearly, the number and location of the band gaps can be tuned by varying the layer thickness of consisting materials. Note that in the calculation, we choose the layer thickness almost at random and optimize a good performance at this range. Thus, it is possible to design another filter performance by tuning block thickness and bias voltage properly. Further, with the growth of the iteration order, the dominant band gaps merely move with a little turbulence at the edge of each band. The turbulence shows a trend of redshift as shown in Fig. 3. This property is universal in

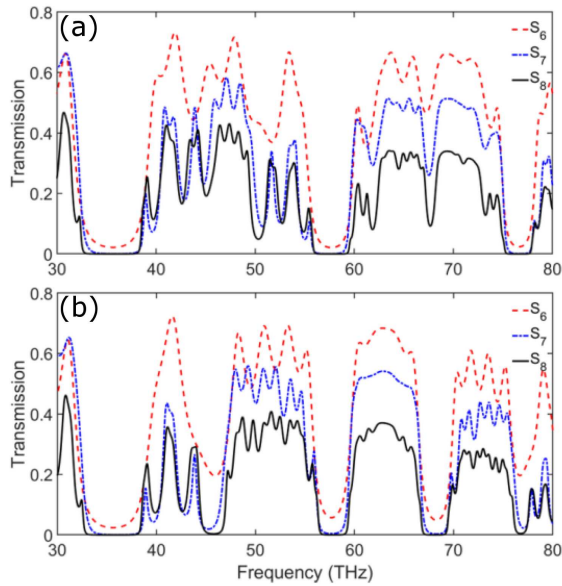


Fig. 3. Transmission spectrum for different generation order of the Fibonacci sequence S_6 , S_7 , and S_8 . The layer thickness is (a) $d_A = 50$ nm and $d_B = 60$ nm and (b) $d_A = 60$ nm and $d_B = 50$ nm, the chemical potential of graphene μ_C is set as 0.7 eV.

a quasiperiodic photonic structure which is known as self-similarity. The self-similar pattern keeps a set of significant characteristics unchanged in the transmission spectrum and changes little in the course of the iterating process. Moreover, the transmission of the GPs decreases significantly from $\sim 60\%$ to $\sim 30\%$ with the evolution of the Fibonacci order from S_6 to S_8 . The reason for transmission declination is mainly the increase of the propagation length of the GPs with the rise of generation order. The S_8 conformation composite $F_8 = 34$ layers while regarding S_6 the layer number is $F_6 = 13$.

The tunable feature of the graphene-based plasmonic filter is demonstrated in Fig. 4. The picture depicts the transmission property of the Fibonacci sequence S_7 in the THz region where a chemical potential varied from 0.5 eV to 0.8 eV. The structure parameters remain unchanged against those calculated in Fig. 3. The red dashed line, blue dash-dotted line, black dotted line and the solid magenta line correspond to the spectrum when μ_C equals 0.5 eV, 0.6 eV, 0.7 eV and 0.8 eV, respectively. For the sake of illustration, we take the logarithm operation to the transmittance. It is evident that the three band gaps of the corresponding chemical potential undertake blueshift for increasing μ_C . The first band gap f_1 altering from 30 THz, to 32 THz, 35 THz and 39 THz corresponds to graphene chemical potential μ_C increase from 0.5 eV to 0.6 eV, 0.7 eV and 0.8 eV, respectively. Similarly, the center of the second band gap f_2 located at 48 THz, 53 THz, 57 THz and 61 THz corresponds to different μ_C ; the mid-frequency of the third

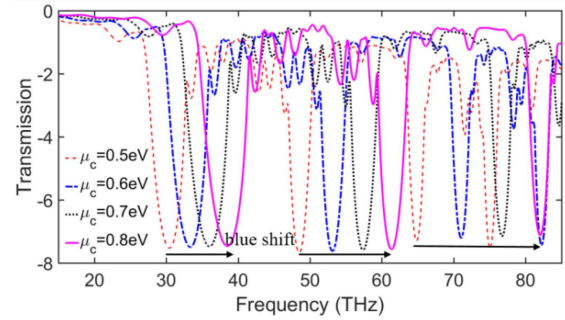


Fig. 4. Transmission spectrum for different chemical potentials of graphene for the Fibonacci sequence S_7 . The chemical potential of graphene μ_C is set to be 0.5 eV, 0.6 eV, 0.7 eV and 0.8 eV. The other parameters remain the same as in Fig. 3.

band gap f_3 transforms from 64 THz to 71 THz, 76 THz and 82 THz, correspondingly. The reason for the blueshift of each band gap can be attributed to the change of the effective refractive index of the building blocks in the DGDS structure which is shown in Fig. 2. The effective refractive index of the DGDS structure is reduced with the increase of graphene chemical potential. Thus, the effective optical length decreases. According to the Bragg condition describing the resonance frequency of periodic structures, we know that the resonance wavelength declines for the reduced optical length. Thus, the blueshift emerges. This result confirms that the principle is still applicable in the case of the Fibonacci quasiperiodic crystals. At the same time, the result also indicates that the proposed structure owns flexible tunability with only little change in the graphene chemical potential μ_C .

In Fig. 5, the transmission property is analyzed for different structure parameters of the consisting layers in the graphene plasmonic filter. It can be seen that the center frequencies of the band gaps are sensitive to the width of the dielectric layer. We investigate the effect of layer thickness d_A on the filter performance in Fig. 5a and the influence of layer thickness d_B on the filter performance in Fig. 5b. In numerical calculation, we choose Fibonacci sequence S_7 , graphene chemical potential $\mu_C = 0.7$ eV in the THz frequency range. In Fig. 5a, the thickness of SiO_2 (d_A) varies from 45 nm to 55 nm while the thickness of TiO_2 layer (d_B) is fixed at 60 nm. With the increase of d_A , the band gaps tend to shift to the lower frequency. The same outcome appears in Fig. 5b, a wider layer thickness of TiO_2 would induce a redshift in the transmission spectrum. Differently from the blueshift caused by increasing chemical potential shown in Fig. 4, the redshift phenomenon appears here. Though, the cause of the redshift is similar to the above discussion — a larger optical length. As a result of the larger optical length induced by increasing layer thickness, the resonance frequency of quasiperiodic photonic crystals tends to decline. Therefore, the

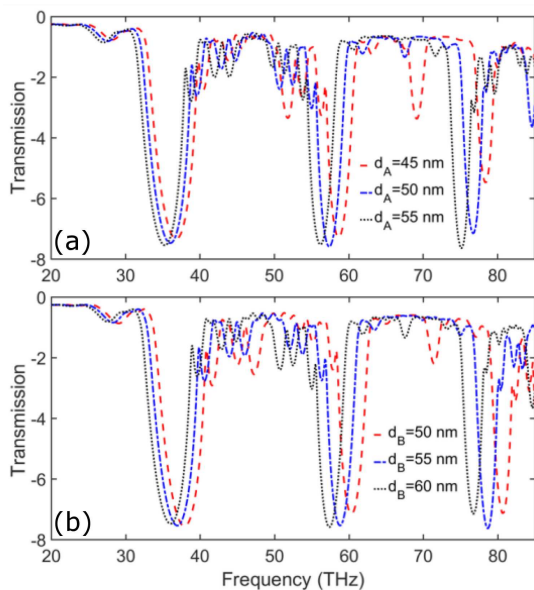


Fig. 5. Transmission spectra for different thickness of layer A (a) and layer B (b) for the Fibonacci sequence S_7 . The thickness of layer A is set as 45 nm, 50 nm and 55 nm and the thickness of the layer B is set as 50 nm, 55 nm and 60 nm.

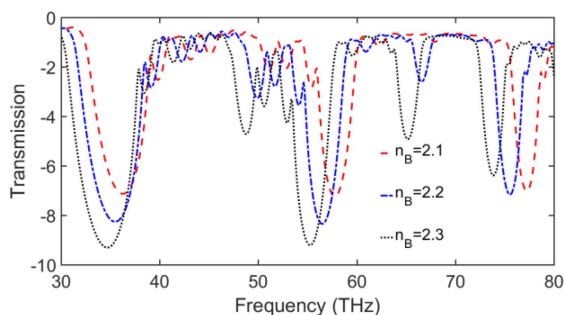


Fig. 6. Transmission spectrum of the Fibonacci sequence S_7 for different refraction indexes of layer B. The refraction index of layer B is set as 2.1, 2.2 and 2.3.

mid-frequencies of the band gaps shift to lower value. Further, we note that to choose a proper thickness of block A and B, we need to take into account the effective index of the GPs. To be more specific, as the effective index shown in Fig. 2 is on the level of ~ 100 , the effective wavelength of GPs is within the scope of (30 nm, 100 nm) for the wavelength within ($3 \mu\text{m}$, $10 \mu\text{m}$). Thus, to get better filter performance, the optical length of block A and B should also be around this range.

Finally, we investigate the influence of the refraction index n_B on the performance of GPs filter with the same structural parameters as those used above. The result is shown in Fig. 6. From (16) and Fig. 2, we can see that the propagation constant β and the effective refractive index n_{eff} of graphene plasmonic is sensitive to the structure geometry. The propagation constant β and the effective refractive index

n_{eff} increase with the growth of the dielectric refraction index n_d . In Fig. 6, the red dashed line denotes $n_B = 2.1$, the blue dash-dotted line denotes $n_B = 2.2$ and the black dotted line denotes $n_B = 2.3$. The transmission spectrum of the multichannel THz plasmonic filter with a different dielectric index indicates that with the increasing of the refraction of n_B , the band gaps tend to redshift just like the result of Fig. 5. The degree of sensitivity displayed in Fig. 6 illustrates that resonant frequency tends to vary 0.1 THz for every 0.1 refractive index change. This result means that we can design a multichannel THz filter corresponding to the specific frequency range. Also, the redshift is due to the increment of the optical length when the dielectric index n_B increases.

4. Conclusions

We propose and analyze a tunable multichannel THz graphene plasmonic filter based on one-dimensional Fibonacci photonic quasicrystals. The transmission properties are calculated in different cases. Both the internal change (structural parameters) and the external variable (graphene chemical potential/gate voltage) can induce a frequency shift in the graphene plasmonic filter. Also, the Fibonacci sequence order is reliable to tune the filter performance. The proposed structure of the GPs filter possesses highly flexible tunability and is sensitive to external changes. Therefore, the proposed structure paves the new way for designing multiple and tunable optical-electrical devices filters, sensors and integrated photonic circuits.

Acknowledgments

This work was supported by the National Natural Science Foundation of China (61801188).

References

- [1] K.S. Novoselov, *Science* **306**, 666 (2004).
- [2] A.K. Geim, K.S. Novoselov, *Nat. Mater.* **6**, 183 (2007).
- [3] H.B. Heersche, P. Jarillo-Herrero, J.B. Oostinga, L.M.K. Vandersypen, A.F. Morpurgo, *Nature* **446**, 56 (2007).
- [4] A. Vakil, N. Engheta, *Science* **332**, 1291 (2011).
- [5] S.S. Sunku, G.X. Ni, B.Y. Jiang et al., *Science* **362**, 1153 (2018).
- [6] B. Shi, W. Cai, X. Zhang, Y. Xiang, Y. Zhan, J. Geng, M. Ren, J. Xu, *Sci. Rep.* **6**, (2016).
- [7] R.R. Nair, P. Blake, A.N. Grigorenko, K.S. Novoselov, T.J. Booth, T. Stauber, N.M.R. Peres, A.K. Geim, *Science* **320**, 1308 (2008).

- [8] Q. Bao, K.P. Loh, *ACS Nano* **6**, 3677 (2012).
- [9] R. Alaei, M. Farhat, C. Rockstuhl, F. Lederer, *Opt. Express* **20**, 28017 (2012).
- [10] Y. Feng, Y. Liu, X. Wang, D. Dong, Y. Shi, L. Tang, *Plasmonics* **13**, 653 (2017).
- [11] K. V. Sreekanth, S. Zeng, K.-T. Yong, T. Yu, *Sens. Actuators B Chem.* **182**, 424 (2013).
- [12] X. Shi, D. Han, Y. Dai, Z. Yu, Y. Sun, H. Chen, X. Liu, J. Zi, *Opt. Express* **21**, 28438 (2013).
- [13] V.P. Gusynin, S.G. Sharapov, J.P. Carbotte, *J. Phys. Condens. Matter* **19**, 026222 (2007).
- [14] F.H.L. Koppens, T. Mueller, Ph. Avouris, A.C. Ferrari, M.S. Vitiello, M. Polini, *Nat. Nanotechnol.* **9**, 780 (2014).
- [15] Q. Bao, H. Zhang, B. Wang, Z. Ni, C.H.Y.X. Lim, Y. Wang, D.Y. Tang, K.P. Loh, *Nat. Photonics* **5**, 411 (2011).
- [16] A.N. Grigorenko, M. Polini, K.S. Novoselov, *Nat. Photonics* **6**, 749 (2012).
- [17] M. Ayata, Y. Fedoryshyn, W. Heni et al., *Science* **358**, 630 (2017).
- [18] J. Chen, M. Badioli, P. Alonso-González et al., *Nature* **487**, 77 (2012).
- [19] L. Ju, B. Geng, J. Horng et al., *Nat. Nanotechnol.* **6**, 630 (2011).
- [20] S.A. Mikhailov, K. Ziegler, *Phys. Rev. Lett.* **99**, 016803 (2007).
- [21] S. Bahadori-Haghighi, R. Ghayour, M.H. Sheikhi, *Carbon* **129**, 653 (2018).
- [22] L. Chen, T. Zhang, X. Li, G. Wang, *Opt. Express* **21**, 28628 (2013).
- [23] B.-H. Huang, W.-B. Lu, X.-B. Li, J. Wang, Z. Liu, *Appl. Opt.* **55**, 5598 (2016).
- [24] J.D. Joannopoulos, S.G. Johnson, J.N. Winn, R.D. Meade, *Photonic Crystals: Molding the Flow of Light*, 2nd ed., Princeton University Press, Princeton 2008.
- [25] U. G. Yasa, Z.G. Figen, H. Kurt, *J. Opt.* **21**, 045101 (2019).
- [26] Y. Fei, Y. Liu, D. Dong, K. Gao, S. Ren, Y. Fan, *Opt. Express* **26**, 34872 (2018).
- [27] X. Wang, Y. Liang, L. Wu, J. Guo, X. Dai, Y. Xiang, *Opt. Lett.* **43**, 4256 (2018).
- [28] D. Dong, Y. Fu, Y. Liu, Y. Fei, Y. Fan, J. Li, Y. Feng, *Appl. Opt.* **58**, 8 (2019).
- [29] J. Hou, H. Wu, D. S. Citrin, W. Mo, D. Gao, Z. Zhou, *Opt. Express* **18**, 10567 (2010).
- [30] M. Kohmoto, B. Sutherland, K. Iguchi, *Phys. Rev. Lett.* **58**, 2436 (1987).
- [31] Z.V. Vardeny, A. Nahata, A. Agrawal, *Nat. Photonics* **7**, 177 (2013).
- [32] E. Maciá, *Rep. Prog. Phys.* **75**, 036502 (2012).
- [33] L. Dal Negro, S.V. Boriskina, *Laser Photonics Rev.* **6**, 178 (2012).
- [34] M.S. Davis, W. Zhu, T. Xu, J.K. Lee, H.J. Lezec, A. Agrawal, *Nat. Commun.* **8**, (2017).
- [35] M. Miscuglio, N.J. Borys, D. Spirito, B. Martín-García, R.P. Zaccaria, A. Weber-Bargioni, P.J. Schuck, R. Krahne, *ACS Nano* **9b**, 00821 (2019).
- [36] D. Zhou, X. Wang, H. Zhu, F. Shen, *Optik* **10**, 281 (2018).
- [37] L. Li, H. Zhao, J. Zhang, H. Hao, F. Xing, *J. Phys. Appl. Phys.* **52**, 255105 (2019).
- [38] S.A. Maier, *Plasmonics: Fundamentals and Applications*, Springer, New York 2007.
- [39] W. Gao, J. Shu, C. Qiu, Q. Xu, *ACS Nano* **6**, 7806 (2012).
- [40] M. Jablan, H. Buljan, M. Soljačić, *Phys. Rev. B* **80**, (2009).
- [41] P.-Y. Chen, A. Alù, *ACS Nano* **5**, 5855 (2011).
- [42] M. Born, E. Wolf, *Principles of Optics: Electromagnetic Theory of Propagation, Interference and Diffraction of Light*, 7th ed. Cambridge University Press, Cambridge 1999.